Original Paper

The neurovascular unit in diffuse intrinsic pontine gliomas

Fatma E. El-Khouly [1,2*], Rianne Haumann [1,2*], Marjolein Breur [3], Sophie E.M. Veldhuijzen van Zanten [1,2], Gertjan J.L. Kaspers [1,2], N. Harry Hendrikse [4,5], Esther Hulleman [1,2], Dannis G. van Vuurden [1,2#], Marianna Bugiani [3#]

[1] *Emma Children's Hospital, Amsterdam UMC – location VUmc, Department of Pediatric Oncology, Cancer Center Amsterdam, de Boelelaan 1117, Amsterdam, The Netherlands*

[2] *Princess Máxima Center for Pediatric Oncology, Utrecht, The Netherlands*

[3] *Amsterdam UMC – location VUmc, Department of Pathology, de Boelelaan 1117, Amsterdam, The Netherlands*

[4] *Amsterdam UMC – location VUmc, Department of Clinical Pharmacology & Pharmacy, de Boelelaan 1117, Amsterdam, The Netherlands*

[5] *Amsterdam UMC – location VUmc, Department of Radiology & Nuclear Medicine, de Boelelaan 1117, Amsterdam, The Netherlands*

[*] *Co-first authorship*

[#] *Co-last authorship*

Corresponding author:
Fatma E. El-Khouly · Amsterdam UMC, Location VUmc · Department of Pediatric Oncology/Hematology · De Boelelaan 1117 · 1081 HV Amsterdam · The Netherlands
f.el-khouly@amsterdamumc.nl

Additional resources and electronic supplementary material: supplementary material

Submitted: 24 April 2021 · Accepted: 27 June 2021 · Copyedited by: Bert M. Verheijen · Published: 5 July 2021

Abstract

Aims: Diffuse intrinsic pontine glioma (DIPG) is a childhood brainstem tumor with a median overall survival of eleven months. Lack of chemotherapy efficacy may be related to an intact blood-brain barrier (BBB). In this study we aim to investigate the neurovascular unit (NVU) in DIPG patients.
Methods: DIPG biopsy (n = 4) and autopsy samples (n = 6) and age-matched healthy pons samples (n = 20) were immunohistochemically investigated for plasma protein extravasation, and the expression of tight junction proteins claudin-5 and zonula occludens-1 (ZO-1), basement membrane component laminin, pericyte marker PDGFR-β, and efflux transporters P-gp and BCRP. The mean vascular density and diameter were also assessed.
Results: DIPGs show a heterogeneity in cell morphology and evidence of BBB leakage. Both in tumor biopsy and autopsy samples, expression of claudin-5, ZO-1, laminin, PDGFR-β and P-gp was reduced compared to healthy pontine tissues. In DIPG autopsy samples, vascular density was lower compared to healthy pons. The density of small vessels (<10 µm) was significantly lower (P<0.001), whereas the density of large vessels (≥10 µm) did not differ between groups (P = 0.404). The median vascular diameter was not significantly different: 6.21 µm in DIPG autopsy samples (range 2.25-94.85 µm), and 6.26 µm in controls (range 1.17-264.77 µm).

Conclusion: Our study demonstrates evidence of structural changes in the NVU in DIPG patients, both in biopsy and autopsy samples, as well as a reduced vascular density in end-stage disease. Adding such a biological perspective may help to better direct future treatment choices for DIPG patients.

Keywords: Diffuse intrinsic pontine glioma (DIPG), Neurovascular unit (NVU), Blood-brain barrier (BBB), Tight junctions, Brainstem, Pons

Introduction

Diffuse intrinsic pontine gliomas (DIPGs) are rare and aggressive childhood malignancies of the brainstem. These tumors are characterized by a diffuse growth pattern closely interwoven within white matter tracts and grey matter structures, and an intrinsic nature, uttered by hypertrophy of the brainstem often encasing the basilar artery [1,2]. With a median overall survival of eleven months, and a two-year survival rate of 10%, DIPGs are the leading cause of brain tumor-related deaths in children [3-7]. In the recent World Health Organization (WHO) classification of tumors of the central nervous system (CNS), DIPGs were reclassified as H3K27M mutated Diffuse Midline Gliomas (DMG H3K27M) [8].

Though much research has been dedicated to DIPG, its poor outcome has remained unchanged for the past 40 years [9]. To date, radiotherapy remains the only (temporarily) effective, albeit palliative treatment, and no chemotherapy regimens prolonging survival have been identified yet. Since *in vitro* and *in vivo* drug testing on patient-derived tumor cells has shown sensitivity to conventional cytotoxic agents and novel drugs, the lack of efficacy in patients is hypothesized to be related to ineffective drug delivery due to an intact blood-brain barrier (BBB) [10-12].

The BBB is formed by endothelial cells interconnected and sealed by tight junctions. The abluminal surface of the endothelium is covered by a basement membrane in which pericytes are embedded. Pericytes control the cerebral blood flow by regulating capillary diameter and vessel stability. The basement membrane is enclosed by astrocyte end-feet, also important for brain homeostasis. Together, pericytes and astrocyte end-feet induce and maintain the integrity of the BBB [13,14]. The BBB regulates transport of essential nutrients to the brain through active transport mechanisms, such as glucose transporters of the GLUT-family. The efflux of waste products and exogenous compounds is mediated through efflux transporters of the ATP-binding cassette family (e.g., P-gp, BCRP, MRP-1) [14,15]. Additionally, the paracellular barrier capacities of the tight junctions limit transport of circulating monoamines and drugs across the BBB [14-16]. The intimate contact and interaction of the BBB complex, formed by endothelial cells, tight junctions, pericytes and astrocyte end-feet, with neurons and perivascular microglia form a dynamic functional unit, called the neurovascular unit (NVU) [13,14,16].

Some studies report different expression of tight junction proteins throughout the brain, suggestive of regional heterogeneity in BBB permeability [17,18]. However, little research has been done on the BBB and NVU in the brainstem and particularly in the pons. Yet, better insight into the BBB and the NVU at these sites is needed to develop new treatment strategies for pediatric brainstem tumors. This especially holds true for DIPG, where the BBB is thought to be a major contributor to therapeutic inefficacy. In this study, we aim at determining and comparing the histological and immunohistochemical characteristics of the NVU of the pons in children with DIPG and age-matched controls.

Patients and Methods

Patients and Samples

DIPG pre-treatment biopsy samples (n = 4) were obtained from the Biobank of the Princess Máxima Center for Pediatric Oncology, Utrecht, the Netherlands, and processed as formalin-fixed paraffin-embedded tissue. End-stage disease DIPG autopsy samples (n = 6) were obtained from the 'VUmc Brain autopsy in children with DIPG' study [19]. This study was approved by the institutional review board of Amsterdam UMC, location VUmc (METc

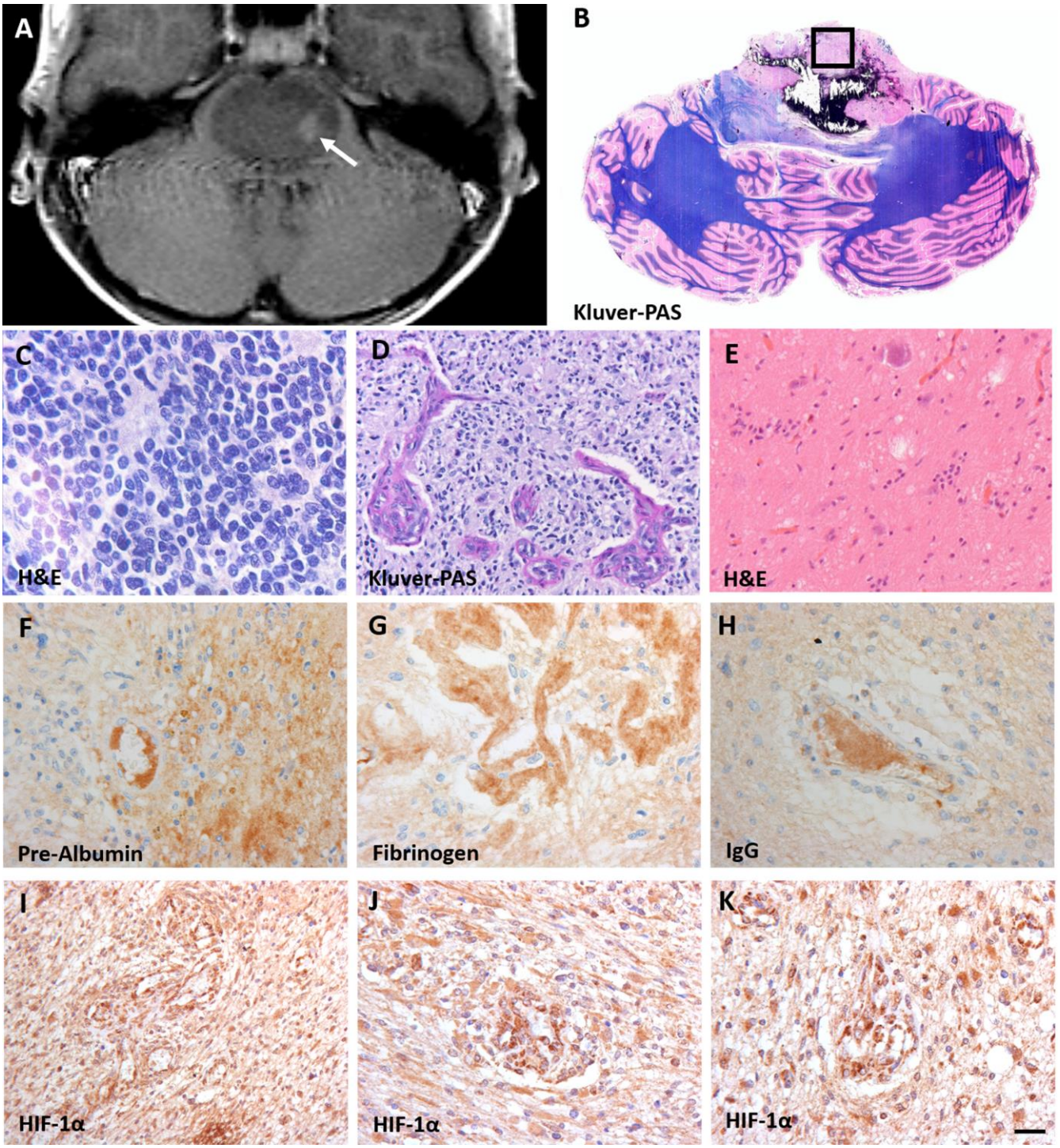

Figure 1: Characteristics of diffuse intrinsic pontine glioma (DIPG). A: T2-weighted MRI-image of a DIPG patient showing an expanded tumor at the basis of the pons. The arrow indicates the biopsy sampling area; **B:** Gross axial section of the pons and cerebellum showing the presence of a diffuse infiltrating tumor in the pons, reaching the middle cerebellar peduncles. The box indicates the sampling location of autopsy tissue at the non-necrotic tumor site; **C-E:** hematoxylin and eosin (H&E) staining of the vital tumor bulk showing morphologic heterogeneity compatible with WHO grade IV tumors **(C and D)** and grade I tumors **(E)**; **F-H:** stains against intravascular plasma proteins pre-albumin **(F)**, fibrinogen **(G)** and IgG **(H)** showing extravasation of these protein into the DIPG tumor parenchyma; **I-K:** hypoxia inducible factor-1α (HIF-1α) staining demonstrating a high expression of HIF-1α. (scale bar: 5 µm)

VUmc, study number: VUMC2009/237) and the Scientific Committee of the Dutch Childhood Oncology Group (DCOG). In this study, brain tissue was obtained within a post-mortem interval of less than six hours for Dutch patients and less than nine hours for patients from abroad, and was processed as formalin-fixed paraffin-embedded tissue or snap frozen. Biopsy samples were MRI-guided and taken from the tumor area displaying the highest hyper-intensity on T2-weighted image (Figure 1A). Autopsy samples were obtained from the non-necrotic tumor core in the pons (Figure 1B).

Age-matched, healthy pontine tissue samples (n = 20) where obtained from the NIH NeuroBioBank, Maryland, United States. Samples were selected based on (i) brain region (pons), (ii) clinical brain diagnosis (unaffected control/sudden deaths), (iii) post-mortem interval (<17 hours), and (iv) presence of formalin-fixed tissue and frozen tissue.

Table 1 shows patient and treatment characteristics of the DIPG patients. Median age at diagnosis was 7.7 years (range 1.3-17.0 years). All patients had a H3K27M mutated DIPG. All autopsy patients,

Table 1: DIPG patient characteristics

Case	Gender	Age at diagnosis (y)	Type of sample	Genetics (WHO grading)	First-line treatment	Second-line treatment	OS (mo.)
1	F	3.5	Biopsy	DMG H3K27M (WHO IV)	n.a.	n.a.	n.a.
2	F	6.9	Biopsy	DMG H3K27M (WHO IV)	n.a.	n.a.	n.a.
3	M	7.9	Biopsy	DMG H3K27M (WHO IV)	n.a.	n.a.	n.a.
4	F	13.6	Biopsy	DMG H3K27M (WHO IV)	n.a.	n.a.	n.a.
5	M	14.4	Autopsy	DMG H3K27M (WHO IV)	RTx	Chemo	18.7
6	F	11.4	Autopsy	DMG H3K27M (WHO IV)	RTx	Chemo	24.0
7	F	17.0	Autopsy	DMG H3K27M (WHO IV)	Chemo-RTx	Chemo	24.7
8	F	1.3	Autopsy	DMG H3K27M (WHO IV)	Chemo	None	10.6
9	F	4.0	Autopsy	DMG H3K27M (WHO IV)	RTx	Chemo-RTx	20.2
10	M	7.5	Autopsy	DMG H3K27M (WHO IV)	RTx	None	5.5

F: female; M: male; y: year; DMG H3K27M: H3K27M mutated diffuse midline glioma; WHO: World Health Organization; RTx: radiotherapy; Chemo-RTx: radiotherapy combined with chemotherapy; OS (mo.): overall survival (months); n.a.: not applicable.

except for the youngest, received radiotherapy at diagnosis. Of these, at disease progression, three out of six received different chemotherapy regimens and two patients did not proceed to further treatment. Median overall survival of patients that were autopsied was 19.5 months (range 5.5-24.0 months). Supplementary Table 1 shows the characteristics of the control group. Median age was 7.0 years (range 1.0-19.0 years). All controls were healthy and had an accidental death.

Immunohistochemistry

Air-dried five-µm-thick cryosections were fixed in 2% formaldehyde for 10 min at room temperature (RT). Aldehyde groups were blocked in 0.1 g glycine in 100 ml distilled water for 10 min at RT. Sections were incubated overnight at RT with a primary antibody: (i) tight junction protein claudin-5 (1:50, Invitrogen, Carlsbad, CA, USA); (ii) tight junction protein ZO-1 (1:50, Invitrogen, Carlsbad, CA, USA); (iii) basement membrane component laminin (1:500, Novus Biologicals, Abingdon UK); or (iv) pericyte marker PDGFR-β (1:500, Abcam, Cambridge, UK). The sections were co-stained with glial fibrillary acidic protein (GFAP; 1:1000, Merck, Darmstadt, Germany). The following day, the sections were incubated with Alexa Fluor®-labelled secondary antibodies, background was quenched with 0.1% Sudan black B, and sections were mounted in mounting medium (Vectashield with 4',6-diamidino-2-fenylindool (DAPI); Vector Laboratories Inc., Burlingame, CA, USA).

Five-µm-thick formalin-fixed paraffin-embedded tissue sections were routinely stained with hematoxylin & eosin (H&E). A gross axial section through the pons and cerebellum was stained with Luxol fast blue-periodic acid-Schiff. For immunohistochemistry, sections were deparaffinized using xylene, and rehydrated through descending alcohol concentrations. Endogenous peroxidase activity was blocked by incubating the slides for 30 min in phosphate buffered saline (PBS) containing 0.3% H_2O_2. Heat-induced antigen retrieval was performed in 0.01 M citrate buffer (pH 6.0). After washing in PBS, the slides were incubated overnight at RT with primary antibodies against P-gp (1:20; Millipore, CA, USA), BCRP (1:40; Abcam, Cambridge, UK), pre-albumin (1:50,000, Dako, Glostrup, Denmark), fibrinogen

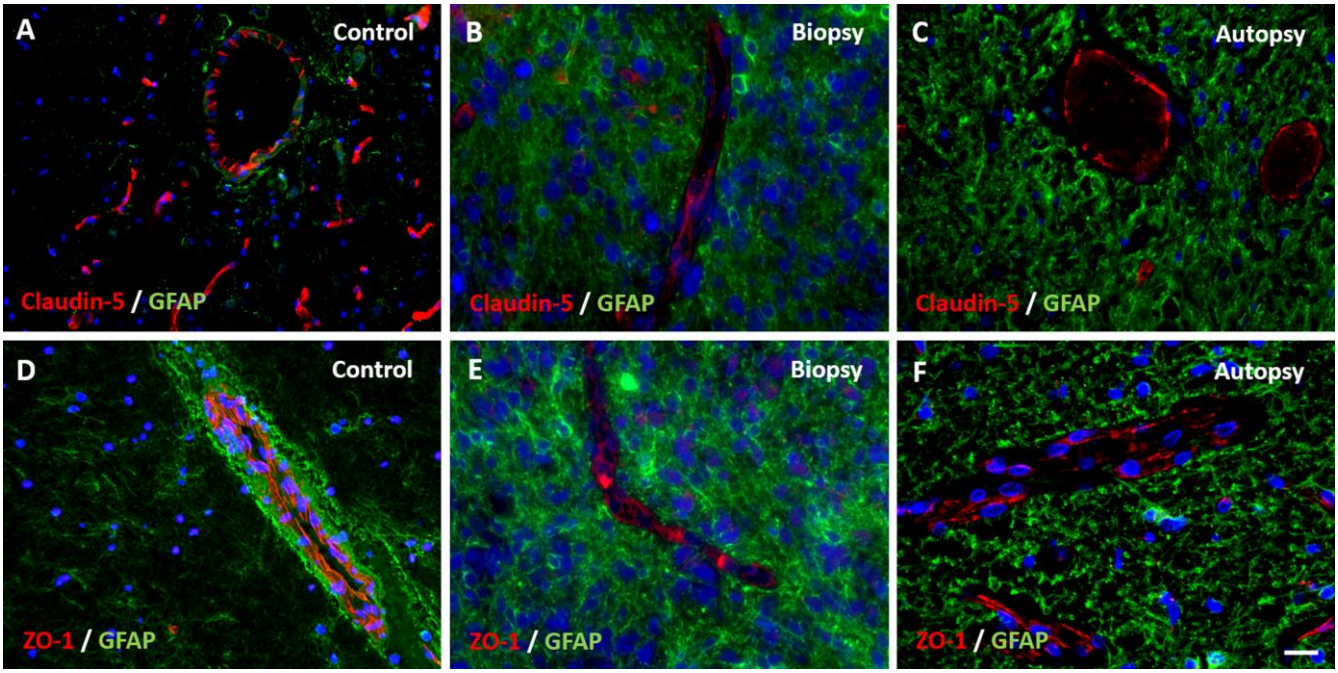

Figure 2: Expression of tight junction proteins claudin-5 and zonula occludens-1 (ZO-1) in DIPG pre-treatment biopsy and post-mortem autopsy samples. In controls, claudin-5 and ZO-1 are sharply defined and have a segmented pattern **(A and D)**. Claudin-5 and ZO-1 show reduced expression in DIPG samples **(B, C, E, F)**. Please note the non-activated state of GFAP-expressing astrocytes in control tissue. (blue: nuclei; green: astrocytes; red: claudin-5 or ZO-1; scale bar: 5 µm)

(1:1,600, Dako, Glostrup, Denmark), IgG (1:800, Dako, Glostrup, Denmark) and hypoxia-inducible factor 1α (HIF-1α; 1:40, Cayman Chemical, Michigan, USA). The next day, slides were incubated with ready-to-use EnVision™-HRP (Dako, Glostrup, Denmark) for 1 hour at RT and visualized with 3,3'Diaminobenzidine (DAB+ DAKO; 1:50, Glostrup, Denmark) for 10 min. The slides were counterstained with hematoxylin for 1 min and mounted with Quick-D mounting medium (Klinipath, Duiven, The Netherlands).

Data analysis

Sections were imaged using a Leica DM6000B microscope (400x magnification; Leica Microsystems BV, Rijswijk, The Netherlands). From each tissue slide, ten images were made. A semi-quantitative analysis of the BBB staining, comparing DIPG samples with control samples, was done by two independent reviewers (FE and RH) using the Leica Application Suite X: LAS X version 3.1.5.16308. The vascular density was assessed on claudin-5-stained tissue sections by counting the number of blood vessels per mm^2. The luminal diameter of the blood vessels was measured with the Leica Application Suite X: LAS X version 3.1.5.16308.

Statistics

Data were analyzed using an independent samples *t*-test (*p*-value = 0.05) using IBM SPSS Statistics version 26. The Levene's Test of Equality of Variance was used to first test the assumption of homogeneity or variance between the groups (*p*-value = 0.05). When equal variances were assumed, pooled estimates were used for the independent *t*-test statistics. When equal variances were not assumed, unpooled data and an adjustment to the degree of freedom (df) were used for the independent *t*-test statistics.

Results

Immunohistochemistry

Figure 1 shows typical DIPG MRI features with enlargement of the pons and contrast enhancement. Gross inspection confirms the presence of a partly necrotic and hemorrhagic tumor center in the pons. Microscopic examination shows variability of tumor cell morphology, ranging from grade I to grade IV according to the 2016 WHO classification of CNS tumors. Tumor areas were recognized based on cell density, the presence of (atypical) mitotic figures and features of high-grade glioma, including necrosis and microvascular proliferation. In these tumors, the integrity of the BBB is compromised, as demonstrated by extravasation of pre-albumin, fibrinogen and IgG. This corresponds with expression of HIF-1α, indicating tumor hypoxia. Notably, as expected for a heterogeneous tumor such as DIPG, the density of GFAP-expressing astrocytes varied throughout the tumor [20]. Additionally, tumor cells were differentiated from pre-existing astrocytes by their higher expression levels of GFAP, conceivably also related to their less differentiated state [20].

Immunohistochemical staining of claudin-5, ZO-1, laminin, PDGFR-β, P-gp and BCRP were evaluable in all samples. Expression of tight junction proteins claudin-5 and ZO-1 was lower at inspection in all DIPG biopsy and autopsy samples compared to control samples (Figure 2). The expression of basement membrane protein laminin was lower at the glial basement membrane in DIPG biopsy and autopsy samples. Interestingly, this was observed in both pre-existent vessels within the tumor cells and in neovascular proliferation (Figure 3). Expression of pericyte marker PDGFR-β was also reduced in both DIPG biopsy and autopsy samples (Figure 4). Efflux transporter P-gp expression was lower in DIPG biopsy and autopsy samples, whereas the expression of BCRP was not different in DIPG compared to controls (Figure 5).

Vascular density

Vascular density per mm^2 was measured in non-necrotic biopsy and autopsy tissue. It was significantly reduced in DIPG autopsy samples compared to controls ($1.5\pm1.2/mm^2$ versus $17.5\pm9.5/mm^2$, respectively; $t_{113,890} = 6.831$, *p*-value <0.001; Figure 6A). Notably, the density of small blood vessels (<10 µm) was significantly lower in DIPG autopsy samples than in controls ($t_{180,609} = -4.303$, *p*-value <0.001), whereas the density of large blood vessels (≥10 µm) did not differ between groups ($t_{597} = -0.835$, *p*-value = 0.404). Most blood vessels in DIPG autopsy and control samples had a

diameter smaller than 10 µm. The median vascular diameter was 6.21 µm in DIPG autopsy samples (range 2.25-94.85 µm), versus 6.26 µm in controls (range 1.17-264.77 µm; Figure 6B). Due to the very small size of the biopsy samples, it was not possible to statistically analyze the vascular density and diameter in these tissue samples. Visual inspection of three patients, however, showed a mean vascular density of 7.5 vessels per mm^2, and a median vascular diameter of 8.23 µm (data not shown).

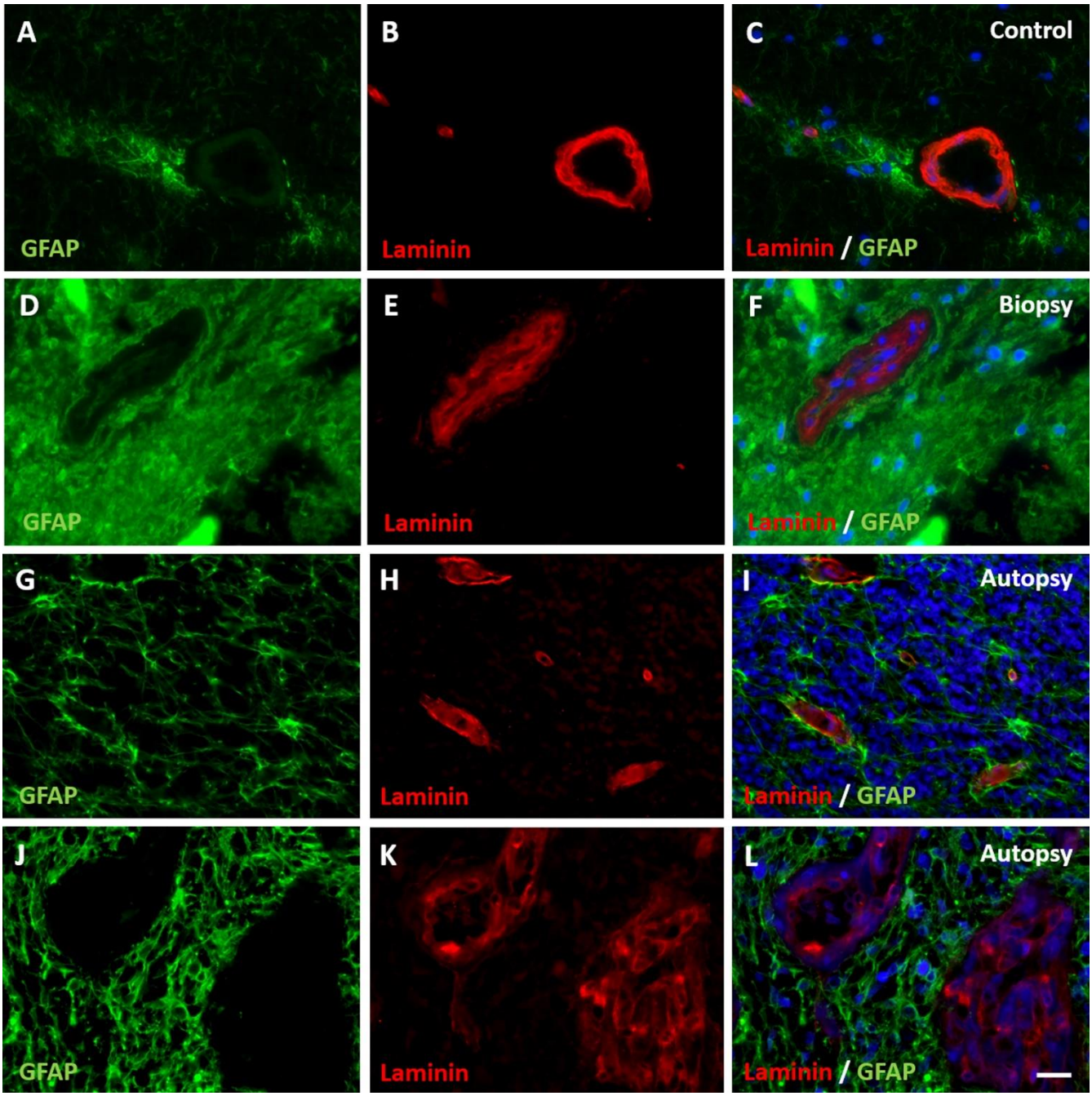

Figure 3: Expression of basement membrane component laminin in DIPG pre-treatment biopsy and post-mortem autopsy samples. In controls **(A-C)**, laminin shows a continuous pattern. Laminin expression was reduced at the glial basement membrane in both DIPG biopsy **(D-F)** and autopsy samples **(G-I)**. This was also observed in neovascularization in autopsy samples **(J-L)**. Of note: neovascular proliferation was not detected in biopsy samples. (blue: nuclei; green: astrocytes; red: laminin; scale bar: 5 µm)

Discussion

Little research has been done to identify the NVU in DIPG, while it is hypothesized that treatment failure is caused by an intact BBB. As summarized by Figure 7, our study demonstrates structural changes in the NVU of DIPG patients that are already present at diagnosis, suggesting these to be tumor-related and not only due to treatment.

All studied DIPG patients harbored a H3K27M mutation, thus fulfilling the diagnosis of DMG H3K27M according to the revised WHO classification [8]. Up to 85% of DIPG patients harbor this mutation [21,22]. Since three out of six DIPG autopsy patients were long-term survivors, the median overall survival of the patients in this group was longer than known from literature, 19.5 months versus 11 months, respectively [7]. Whether neuropathological grading (WHO II-IV), tumor location or the presence of a H3K27M mutation have an impact on survival is still not clear [22-24].

The barrier properties of the NVU strongly depend on the complex interaction between endothelial cells and their tight junctions, pericytes, basement membranes and astrocytes. In physiological conditions, tight junctions are formed by inter-endothelial connections between transmembrane proteins of the claudin-family (claudin-1, 3, 5, and 12), which regulate the function of these tight junctions[25,26]. Claudins are anchored into the endothelial cells by proteins from the zonula occludens-family (ZO-1, 2, and 3) that regulate adherens junctions and influence cytoskeletal organization, angiogenic potential and cell migration [27]. Moreover, ZO-1 is

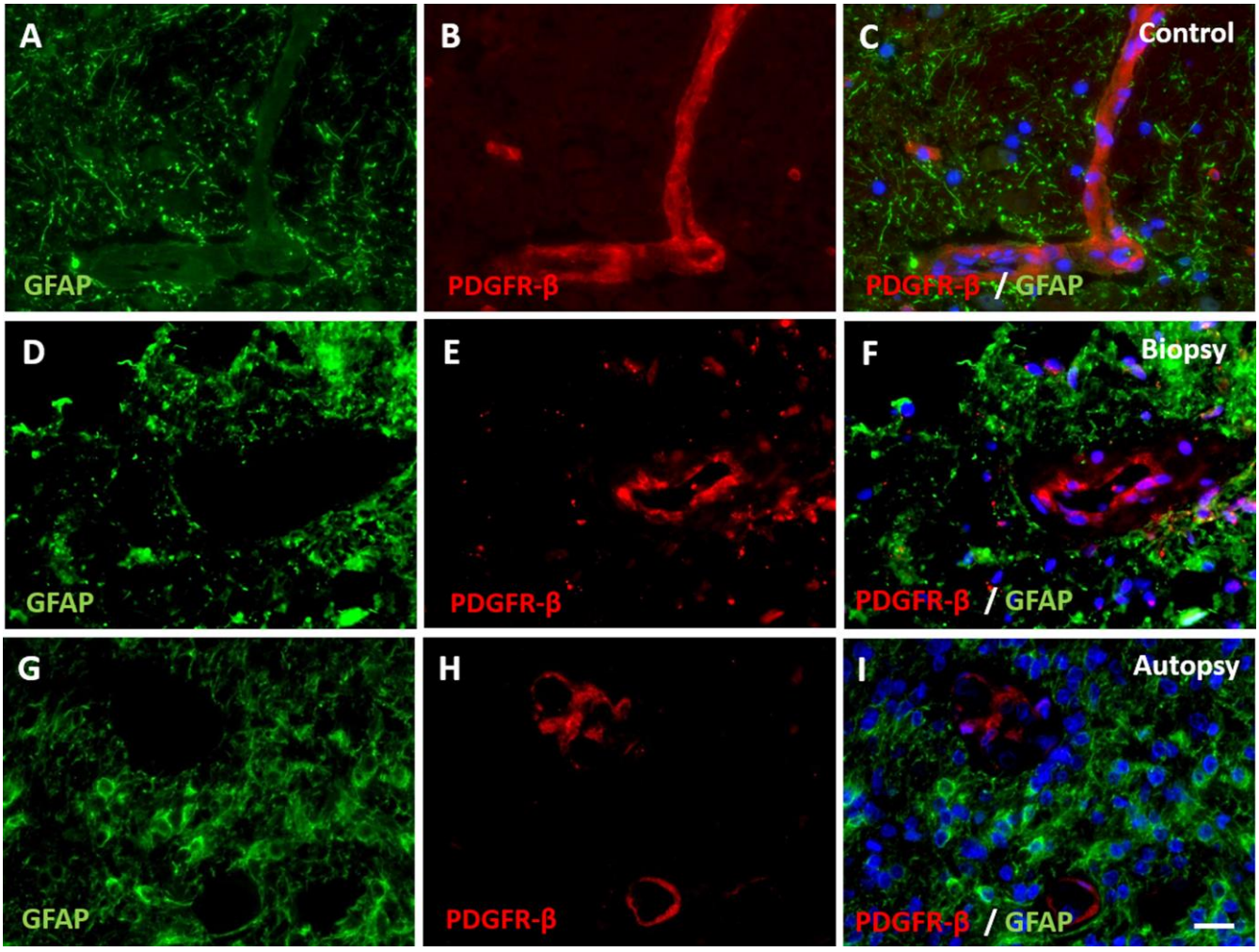

Figure 4: Expression of pericyte marker PDGFR-β in DIPG pre-treatment biopsy and post-mortem autopsy samples. In controls **(A-C)**, PDGFR-β shows a continuous pattern. Expression of PDGFR-β was reduced in both DIPG biopsy **(D-F)** and autopsy samples **(G-I)**. (blue: nuclei; green: astrocytes; red: PDGFR-β; scale bar: 5 µm).

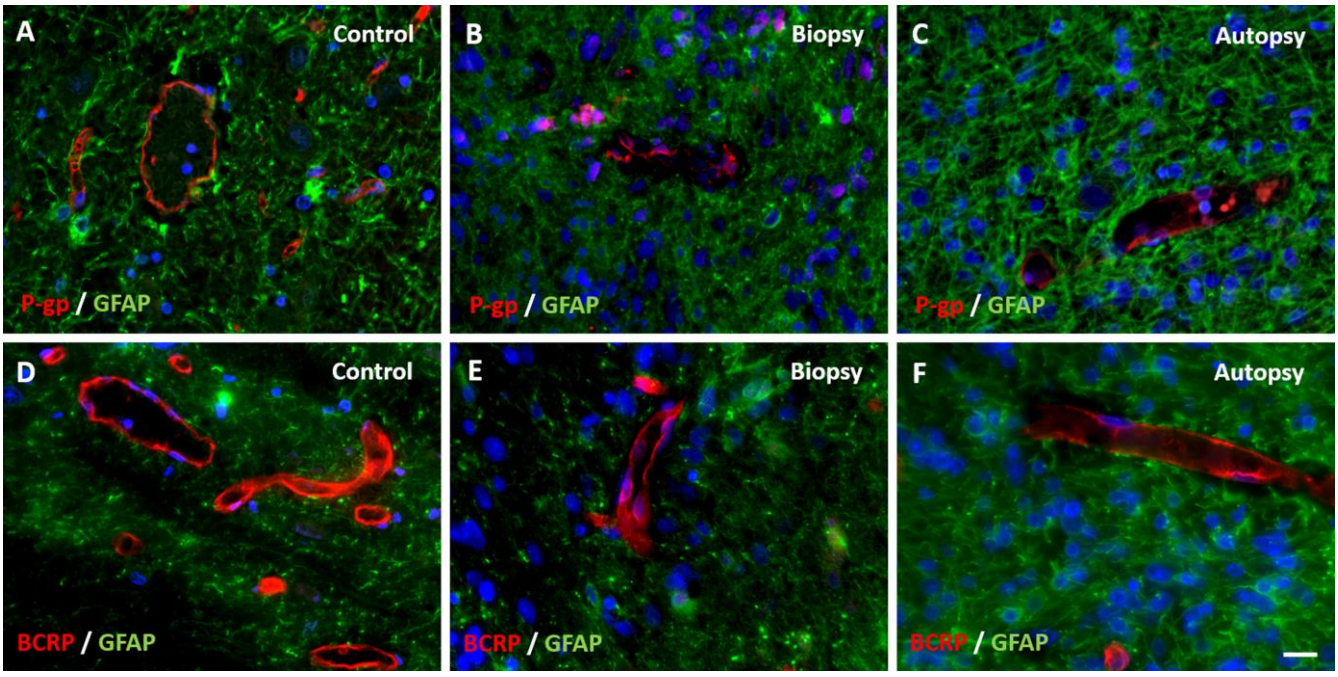

Figure 5: Expression of efflux transporters P-gp and BCRP in DIPG pre-treatment biopsy and post-mortem autopsy samples. P-gp and BCRP are sharply defined and have a segmented pattern in controls **(A and D)**. Expression of P-gp was reduced in both DIPG samples **(B and C)**. BCRP expression was unchanged in DIPG samples **(E and F)**. (blue: nuclei; green: astrocytes; red: P-gp or BCRP; scale bar: 5 µm)

responsible for the spatial organization of claudin-5 by linking it to the actin cytoskeleton [25]. Downregulation of ZO-1 can lead to tight junction disruption and a larger intercellular distance between endothelial cells and thus pathologically increased paracellular transport [27]. Claudin-5 is most abundant in brain vessels (600-times higher expression than other claudins), where it has a heterogeneous distribution [26]. The highest claudin-5 expression is seen in capillaries and small post-capillary venules [25,28]. In a claudin-5 knockout mouse model, an increased leakage of molecules up to 800 Da was observed [29], whereas the permeability of normal BBB only allows passage of molecules up to 500 Da [30,31]. When additional tight junction proteins are downregulated, a size-dependent increase in paracellular transport is seen of molecules with a size up to 10,000 Da [29,32]. In our study, a reduced expression of claudin-5 and ZO-1 was observed in DIPG patients both pre-treatment and post-mortem, indicating a barrier defect, and increasing paracellular transport across the BBB [27]. Nevertheless, there are more tight junction proteins of the zonula occludens and claudin-family expressed by brain endothelial cells. Whether possible downregulation of claudin-5 and ZO-1 is compensated by overexpression of other tight junction proteins remains unknown.

Endothelial cells are surrounded by a basement membrane that contains laminin produced by pericytes and astrocytes [33,34]. Laminin is essential for basement membrane assembly and maintenance of NVU integrity [35]. In our study, employing a pan-laminin antibody, we found that expression of laminin was lower at the glial basement membrane in both DIPG biopsy and autopsy samples. This was observed in pre-existent vessels amongst the tumor cells and in neovascular proliferation. Our results suggest a pathological involvement of pericytes and astrocytes in DIPG that could have consequences on the behavior of the endothelial cells, thus also disrupting the integrity of the NVU [34]. Immunohistochemistry showed also a lower expression of PDGFR-β in DIPG biopsy and autopsy samples, suggesting a reduction in pericytic coverage in DIPG NVU. Besides contributing to secretion of basement membrane components [33,34], pericytes are essential for regulating capillary diameter and vessel stability [13]. The possible reduction of pericytic coverage observed in our study may explain the possible downregulation of laminin at the glial basement membrane in DIPG patients.

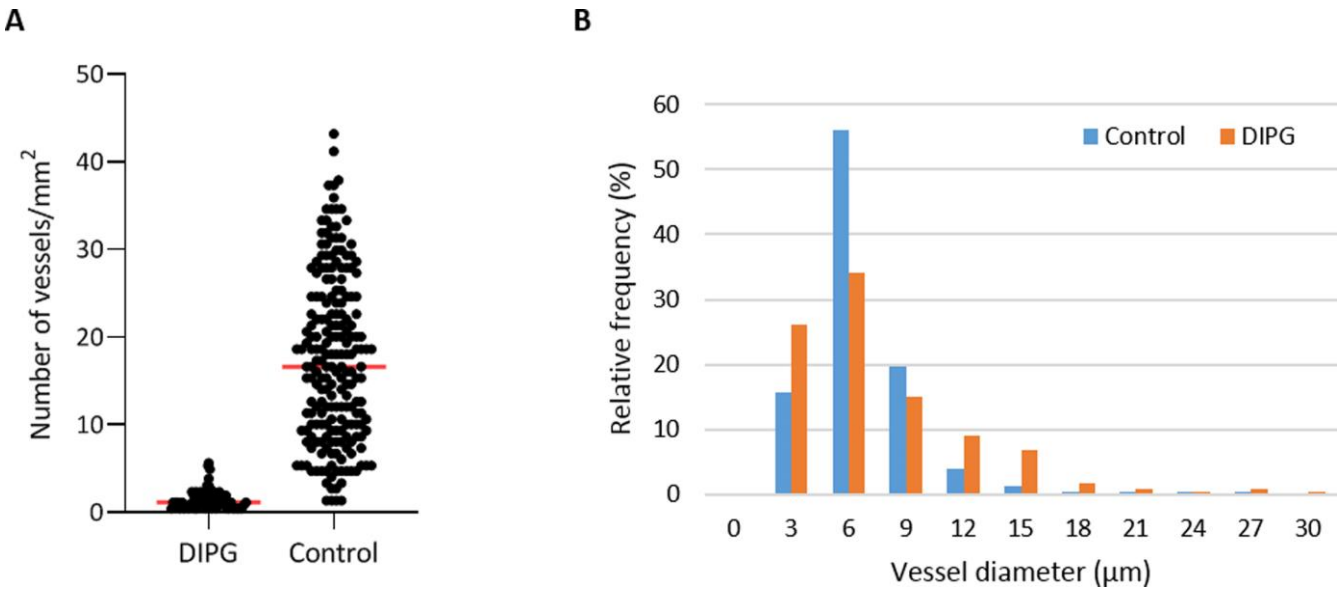

Figure 6: Vascular density and diameter in DIPG post-mortem autopsy and healthy control samples. A: vascular density in DIPG post-mortem autopsy samples and healthy control samples. Mean vascular density was 1.5±1.2/mm² in DIPG versus 17.5±9.5/mm² in controls (red line). **B:** Vascular size distribution in DIPG post-mortem samples and healthy control samples.

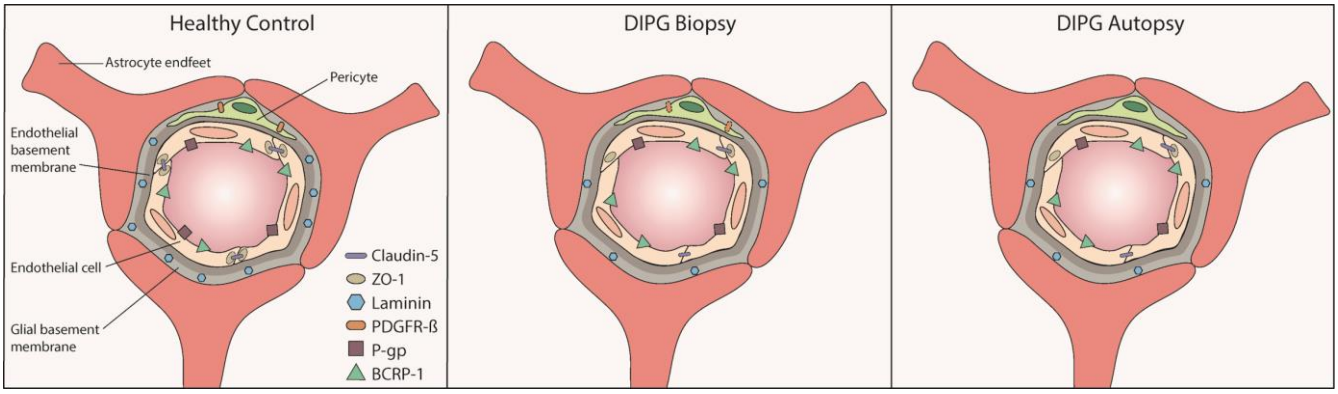

Figure 7: Graphical overview of the structural capillary changes observed in DIPG pre-treatment biopsy and post-mortem autopsy samples: lower expression of tight junction proteins claudin-5 and ZO-1, basement membrane component laminin, pericyte marker PDGFR-β and efflux transporter P-gp in DIPG biopsy and autopsy samples; unchanged expression of efflux transporter BCRP-1 in DIPG biopsy and autopsy samples.

Under physiological conditions, P-gp and BCRP are the most dominantly expressed efflux transporters in de BBB [36,37]. Our study shows a decreased P-gp expression and unchanged BCRP expression in DIPG pre-treatment and post-mortem samples. This is in line with previous work showing a "moderate expression" of P-gp and intense staining of BCRP in DIPG tumor vasculature [10].

Overall, our results show alterations of the NVU in DIPG patients, which could result in or reflect a more leaky NVU. This hypothesis of a leaky NVU is supported by the demonstrated extravasation of some intravascular proteins, such as pre-albumin, fibrinogen and IgG. Theoretically, this might positively influence influx of chemotherapeutic agents into the tumor, based on passive diffusion. Clinical data, however, do not support this possibility [38,39]. A possible explanation for this discrepancy might be the markedly reduced vascular density in DIPG that could overrule the effects of a leaky NVU. Whether the reduction of vascular density is also present at diagnosis remains to be investigated.

Lack of therapy efficacy in DIPG has been linked to an intact BBB. Here, we demonstrated structural changes of the NVU together with a lower vascular density in these tumors. These findings have consequences for drug administration, since coverage of the whole tumor, including the migrating/diffusely growing tumor cells, is essential. Our findings suggest that drug administration techniques that mostly rely on vascular density for drug distribution, including conventional systemic administration and microbubble mediated focused ultrasound, might show limited efficacy in DIPG [12]. In contrast, convection-enhanced delivery might be a more suitable technique, in which drug distribution across the tumor relies on a positive pressure gradient instead of passive diffusion [12,40,41]. Adding such a biological NVU perspective may help to better direct treatment choices for DIPG patients in the future.

Acknowledgement

We thank the employees of the Expertise Center for Post-mortem Diagnostics of the Amsterdam University Medical Centers, location VUmc, for assisting with the autopsies of the DIPG patients. We also thank the NIH NeuroBiobank for providing the control tissue. We would also like to thank the Semmy Foundation (Stichting Semmy) for financially supporting DIPG research in the Amsterdam University Medical Centers, location VUmc.

Ethical Approval

The study was approved by the Medical ethical committee of the Amsterdam University Medical Center, location VUmc (METc VUmc, study number VUMC2009/237). This study was conducted in accordance to the declaration of Helsinki.

Data Sharing and Data Accessibility

The data that support the findings of this study are available from the corresponding author upon reasonable request.

References

1. Epstein F, McCleary EL. Intrinsic brain-stem tumors of childhood: surgical indications. *J Neurosurg* 1986; **64**(1): 11-5.
2. Yoshimura J, Onda K, Tanaka R, Takahashi H. Clinicopathological study of diffuse type brainstem gliomas : analysis of 40 autopsy cases. *Neurol Med Chir (Tokyo)* 2003; **43**: 375-82.
3. Broniscer A, Gajjar A. Supratentorial high-grade astrocytoma and diffuse brainstem glioma: two challenges for the pediatric oncologist. *Oncologist* 2004; **9**(2): 197-206.
4. Hargrave D, Bartels U, Bouffet E. Diffuse brainstem glioma in children: critical review of clinical trials. *The lancet oncology* 2006; **7**(3): 241-8.
5. Jansen MH, Veldhuijzen van Zanten SE, Sanchez Aliaga E, et al. Survival prediction model of children with diffuse intrinsic pontine glioma based on clinical and radiological criteria. *Neuro Oncol* 2015; **17**(1): 160-6.
6. Veringa SJE, Biesmans D, van Vuurden DG, et al. In vitro drug response and efflux transporters associated with drug resistance in pediatric high grade glioma and diffuse intrinsic pontine glioma. *PloS one* 2013; **8**(4): e61512-e.
7. Hoffman LM, Veldhuijzen van Zanten SEM, Colditz N, et al. Clinical, Radiologic, Pathologic, and Molecular Characteristics of Long-Term Survivors of Diffuse Intrinsic Pontine Glioma (DIPG): A Collaborative Report From the International and European Society for Pediatric Oncology DIPG Registries. *Journal of Clinical Oncology* 2018; **36**(19): 1963-72.
8. Louis DN, Perry A, Reifenberger G, et al. The 2016 World Health Organization Classification of Tumors of the Central Nervous System: a summary. *Acta Neuropathol* 2016; **131**(6): 803-20.
9. Sewing AC, Caretti V, Lagerweij T, et al. Convection enhanced delivery of carmustine to the murine brainstem: a feasibility study. *J Neurosci Methods* 2014; **238**: 88-94.
10. Veringa SJ, Biesmans D, van Vuurden DG, et al. In vitro drug response and efflux transporters associated with drug resistance in pediatric high grade glioma and diffuse intrinsic pontine glioma. *PLoS One* 2013; **8**(4): e61512.
11. Grasso CS, Tang Y, Truffaux N, et al. Functionally defined therapeutic targets in diffuse intrinsic pontine glioma. *Nat Med* 2015; **21**(6): 555-9.
12. Haumann R, Videira JC, Kaspers GJL, van Vuurden DG, Hulleman E. Overview of Current Drug Delivery Methods Across the Blood-Brain Barrier for the Treatment of Primary Brain Tumors. *CNS Drugs* 2020; **34**(11): 1121-31.
13. Obermeier B, Daneman R, Ransohoff RM. Development, maintenance and disruption of the blood-brain barrier. *Nat Med* 2013; **19**(12): 1584-96.
14. Serlin Y, Shelef I, Knyazer B, Friedman A. Anatomy and physiology of the blood-brain barrier. *Semin Cell Dev Biol* 2015; **38**: 2-6.
15. Abbott NJ, Ronnback L, Hansson E. Astrocyte-endothelial interactions at the blood-brain barrier. *Nat Rev Neurosci* 2006; **7**(1): 41-53.

16. Liebner S, Dijkhuizen RM, Reiss Y, Plate KH, Agalliu D, Constantin G. Functional morphology of the blood-brain barrier in health and disease. *Acta Neuropathol* 2018; **135**(3): 311-36.

17. Wilhelm I, Nyul-Toth A, Suciu M, Hermenean A, Krizbai IA. Heterogeneity of the blood-brain barrier. *Tissue Barriers* 2016; **4**(1): e1143544.

18. Villabona-Rueda A, Erice C, Pardo CA, Stins MF. The Evolving Concept of the Blood Brain Barrier (BBB): From a Single Static Barrier to a Heterogeneous and Dynamic Relay Center. *Front Cell Neurosci* 2019; **13**: 405.

19. Caretti V, Jansen MH, van Vuurden DG, et al. Implementation of a multi-institutional diffuse intrinsic pontine glioma autopsy protocol and characterization of a primary cell culture. *Neuropathol Appl Neurobiol* 2013; **39**(4): 426-36.

20. Bugiani M, Veldhuijzen van Zanten SEM, Caretti V, et al. Deceptive morphologic and epigenetic heterogeneity in diffuse intrinsic pontine glioma. *Oncotarget* 2017; **8**(36): 60447-52.

21. Castel D, Philippe C, Calmon R, et al. Histone H3F3A and HIST1H3B K27M mutations define two subgroups of diffuse intrinsic pontine gliomas with different prognosis and phenotypes. *Acta Neuropathol* 2015; **130**(6): 815-27.

22. Karremann M, Gielen GH, Hoffmann M, et al. Diffuse high-grade gliomas with H3 K27M mutations carry a dismal prognosis independent of tumor location. *Neuro Oncol* 2018; **20**(1): 123-31.

23. Wagner S, Warmuth-Metz M, Emser A, et al. Treatment options in childhood pontine gliomas. *J Neurooncol* 2006; **79**(3): 281-7.

24. von Bueren AO, Karremann M, Gielen GH, et al. A suggestion to introduce the diagnosis of "diffuse midline glioma of the pons, H3 K27 wildtype (WHO grade IV)". *Acta Neuropathol* 2018; **136**(1): 171-3.

25. Greene C, Hanley N, Campbell M. Claudin-5: gatekeeper of neurological function. *Fluids Barriers CNS* 2019; **16**(1): 3.

26. Jia W, Lu R, Martin TA, Jiang WG. The role of claudin-5 in blood-brain barrier (BBB) and brain metastases (review). *Mol Med Rep* 2014; **9**(3): 779-85.

27. Tornavaca O, Chia M, Dufton N, et al. ZO-1 controls endothelial adherens junctions, cell-cell tension, angiogenesis, and barrier formation. *J Cell Biol* 2015; **208**(6): 821-38.

28. Paul D, Cowan AE, Ge S, Pachter JS. Novel 3D analysis of Claudin-5 reveals significant endothelial heterogeneity among CNS microvessels. *Microvasc Res* 2013; **86**: 1-10.

29. Nitta T, Hata M, Gotoh S, et al. Size-selective loosening of the blood-brain barrier in claudin-5-deficient mice. *J Cell Biol* 2003; **161**(3): 653-60.

30. El-Khouly FE, van Vuurden DG, Stroink T, et al. Effective Drug Delivery in Diffuse Intrinsic Pontine Glioma: A Theoretical Model to Identify Potential Candidates. *Front Oncol* 2017; **7**: 254.

31. Pike VW. PET radiotracers: crossing the blood-brain barrier and surviving metabolism. *Trends in pharmacological sciences* 2009; **30**(8): 431-40.

32. Keaney J, Walsh DM, O'Malley T, et al. Autoregulated paracellular clearance of amyloid-β across the blood-brain barrier. *Science Advances* 2015; **1**(8): e1500472.

33. Gautam J, Zhang X, Yao Y. The role of pericytic laminin in blood brain barrier integrity maintenance. *Sci Rep* 2016; **6**: 36450.

34. Yao Y, Chen ZL, Norris EH, Strickland S. Astrocytic laminin regulates pericyte differentiation and maintains blood brain barrier integrity. *Nat Commun* 2014; **5**: 3413.

35. Givant-Horwitz V, Davidson B, Reich R. Laminin-induced signaling in tumor cells. *Cancer Lett* 2005; **223**(1): 1-10.

36. Al-Majdoub ZM, Al Feteisi H, Achour B, et al. Proteomic Quantification of Human Blood-Brain Barrier SLC and ABC Transporters in Healthy Individuals and Dementia Patients. *Mol Pharm* 2019; **16**(3): 1220-33.

37. Uchida Y, Ohtsuki S, Katsukura Y, et al. Quantitative targeted absolute proteomics of human blood-brain barrier transporters and receptors. *J Neurochem* 2011; **117**(2): 333-45.

38. El-Khouly FE, Veldhuijzen van Zanten SEM, Santa-Maria Lopez V, et al. Diagnostics and treatment of diffuse intrinsic pontine glioma: where do we stand? *J Neurooncol* 2019; **145**(1): 177-84.

39. Veldhuijzen van Zanten SE, Jansen MH, Sanchez Aliaga E, van Vuurden DG, Vandertop WP, Kaspers GJ. A twenty-year review of diagnosing and treating children with diffuse intrinsic pontine glioma in The Netherlands. *Expert Rev Anticancer Ther* 2015; **15**(2): 157-64.

40. Barua NU, Hopkins K, Woolley M, et al. A novel implantable catheter system with transcutaneous port for intermittent convection-enhanced delivery of carboplatin for recurrent glioblastoma. *Drug Deliv* 2016; **23**(1): 167-73.

41. Lewis O, Woolley M, Johnson D, et al. Chronic, intermittent convection-enhanced delivery devices. *J Neurosci Methods* 2016; **259**: 47-56.